A Comprehensive Model for Control of Vaporizing Liquid Microthrusters

Silva, Marsil A.C.; Silvestrini, Stefano; Guerrieri, Dadui C.; Cervone, Angelo; Gill, Eberhard

DOI
10.1109/TCST.2018.2865789

Publication date
2018

Document Version
Accepted author manuscript

Published in
IEEE Transactions on Control Systems Technology

A Comprehensive Model for Control of Vaporizing Liquid Microthrusters

Marsil A. C. Silva, Stefano Silvestrini, Daduí C. Guerrieri, Angelo Cervone, and Eberhard Gill

***Abstract*— This brief presents a comprehensive approach for the modeling of micropropulsion systems based on the vaporization of a liquid. The model combines the analytical and empirical relations derived from extensive experimental analysis and fundamental physical laws. This allows modeling of key parameters, such as mass flow rate, for the entire system comprising a tank to store the liquid propellant, a valve to control the mass flow, and a microthruster that vaporizes the propellant and accelerates it generating thrust. The model is evaluated by a sensitivity analysis considering the boundaries of the modeling space, and it has been tested in a simulation loop demonstrating the attitude control of a nanosatellite using a set of four thrusters. The results of the simulation are used to test the developed model.**

***Index Terms*— Control, modeling, spacecraft, vaporizing liquid microthruster (VLM).**

I. Introduction

MICROPROPULSION systems have been recognized as one of the key features to be developed for the next generation of space missions using very small spacecraft, including modular concepts such as CubeSats and PocketQubes [1]. These satellites are based on form factors called units that can be stacked together to combine several different modules.

A micropropulsion system is able to provide thrust in the levels from nanonewtons to micronewtons, which perfectly matches the requirements imposed by these classes of satellites. The integration of such a device into the bus of the spacecraft will represent a great technological advancement allowing them to execute precise attitude control or orbital maneuvers, thus extending the range of application of these spacecraft to include missions that involve space debris removal, orbit transfer, and so on [2], [3].

Many concepts of micropropulsion have been proposed during the last decades; especially, systems that are manufactured using microelectromechanical systems (MEMS) fabrication technologies have received great attention [4]. An interesting option for CubeSats and PocketQubes is the vaporizing liquid microthrusters (VLMs) that use a resistive heater to heat up the propellant and eject it through a nozzle. The VLM has received attention due to its ability to provide high thrust levels with relatively low power consumption.

Manuscript received October 5, 2017; revised March 28, 2018 and June 28, 2018; accepted August 6, 2018. Manuscript received in final form August 13, 2018. This work was supported by the Conselho Nacional de Desenvolvimento Científico e Tecnológico, Brazil. Recommended by Associate Editor X. Chen. *(Corresponding author: Marsil A. C. Silva.)*

The authors are with the Space Engineering Department, Faculty of Aerospace Engineering, Delft University of Technology, 2629 HS Delft, The Netherlands (e-mail: m.deathaydecostaesilva@tudelft.nl).

Color versions of one or more of the figures in this paper are available online at http://ieeexplore.ieee.org.

Digital Object Identifier 10.1109/TCST.2018.2865789

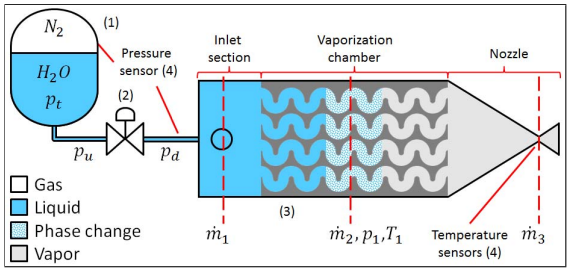

Fig. 1. VLM system showing: 1) a tank; 2) a valve; 3) a thruster, and 4) sensors. The mass flow rate $\dot{m}_1$ is the liquid flow rate, $\dot{m}_2$ is the vaporization rate, and $\dot{m}_3$ is the mass flow of the nozzle.

Although the development of VLM systems has been quite significant, the modeling of such a system is limited to relations of power and thrust and cover only the steady-state behavior [5], [6]. A model that reproduces the dynamic behavior of the system is very important for the design of controllers to allow the precise operation of the thruster and also for the design of the entire spacecraft.

In this brief, we present a comprehensive model of the VLM combining analytical and empirical relations and including models of all the components of a VLM system. The model allows the simulation of the complete system, including particularities involved in the process such as temperature and pressure changes caused by the operation of the thruster. The system considered is composed by a tank to store the propellant, a valve to control the liquid flow, and a thruster to vaporize the liquid and generate thrust. The thruster is designed to work with water as the propellant, since it has been shown that water is a very good candidate for this kind of propulsion system due to its density that results in higher Δv (change in velocity) per volume of propellant when compared with other safe substances [7].

A. Background

1) Vaporizing Liquid Microthruster: Fig. 1 shows a diagram of a complete VLM system [8]. The liquid propellant enters through the inlet section to the vaporization chamber, where it is vaporized by applying power to resistive heaters attached to the walls of the thruster. A convergent–divergent nozzle accelerates the vapor to supersonic velocities.

2) Propulsion: The performance of micropropulsion systems can generally be analyzed using the same formulation as in the normal sized systems. In this case, two parameters are of major interest when analyzing the performance of the thruster: specific impulse and thrust. The thrust F is the force generated by the gas accelerated and expelled through the nozzle [9]

$$F = \dot{m} v_e + (p_e - p_a) A_e \tag{1}$$

where $\dot{m}$ is the mass flow rate, v_e is the exhaust velocity, p_e and p_a are the exit and ambient pressures, and A_e is the exit area of the nozzle. The exhaust velocity can be calculated by (2), where M_e is the Mach number at the exit, γ is the ratio of the specific heat at constant pressure and constant volume, T_e is the exit temperature, and R_s is the specific gas constant

$$v_e = M_e\sqrt{\gamma\, R_s T_e}. \tag{2}$$

The mass flow rate $\dot{m}$ can be written as a function of the chamber (stagnation) pressure and temperature (p_1 and T_1) and the area of the throat A_t

$$\dot{m} = \frac{A_t p_1}{\sqrt{T_1}}\sqrt{\frac{\gamma}{R_s}\left(\frac{2}{\gamma+1}\right)^{\frac{\gamma+1}{\gamma-1}}}. \tag{3}$$

Equations (4)–(6) are used to calculate the Mach number, temperature, and pressure at the exit

$$\frac{A_e}{A_t} = \left(\frac{\gamma+1}{2}\right)^{-\frac{\gamma+1}{2(\gamma-1)}} M_e^{-1}\left(1+\frac{\gamma-1}{2}M_e^2\right)^{\frac{\gamma+1}{2(\gamma-1)}} \tag{4}$$

$$T_e = T_1\left(1+\frac{(\gamma-1)}{2}{M_e}^2\right)^{-1} \tag{5}$$

$$p_e = p_1\left(1+\frac{(\gamma-1)}{2}{M_e}^2\right)^{\frac{-\gamma}{\gamma-1}}. \tag{6}$$

The specific impulse I_{sp} is a measure of efficiency regarding the consumption of propellant

$$I_{sp} = \frac{\int_0^t F dt}{g\int_0^t \dot{m} dt} \tag{7}$$

where $g = 9.80665\ \mathrm{ms}^{-2}$ is the gravitational acceleration on the earth at sea level.

3) Attitude Dynamics: Assuming the spacecraft as a rigid body, we can describe its angular acceleration by the following equation:

$$\dot{\vec{\omega}} = I^{-1}[-(\vec{\omega}\times I\vec{\omega}) + \vec{M}_{\text{ext}}] \tag{8}$$

where $\vec{\omega}$ is the angular velocity of the body, I is the inertia matrix, and $\vec{M}_{\text{ext}}$ is any external torque. In an ideal case where no disturbances are considered, $\vec{M}_{\text{ext}}$ is the torque provided by the actuators on board of the spacecraft. In this brief, the spacecraft is equipped with four thrusters positioned in such a way to provide torques in any direction with respect to the center of mass that is coincident with the geometric center of the spacecraft, as shown in Fig. 2.

The total torque of N thrusters is calculated based on the position $\vec{d}$ and the orientation $\vec{e}$ of each thruster i

$$\vec{M}_{\text{ext}} = \sum_{i=1}^{N}([\vec{d}_i\times\vec{e}_i]F_i). \tag{9}$$

The attitude of the spacecraft with respect to any arbitrary reference frame can be represented using quaternions. Using the angular velocity defined in (8), we can calculate the change in the attitude represented in quaternions q [10]

$$\dot{q} = \begin{bmatrix} 0 & -\omega_x & -\omega_y & -\omega_z \\ \omega_x & 0 & \omega_z & -\omega_y \\ \omega_y & -\omega_z & 0 & \omega_x \\ \omega_z & \omega_y & -\omega_x & 0 \end{bmatrix} q \tag{10}$$

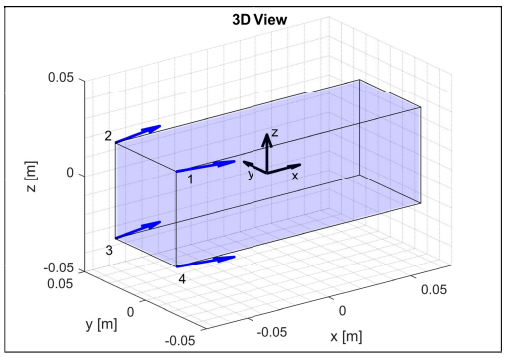

Fig. 2. 3-D model of the spacecraft used in the simulations. Blue arrows: position and direction of the thrusters. Black arrows: center of mass and the reference frame.

where ω_x, ω_y, and ω_z are the components of the vector $\vec{\omega}$. By knowing the initial attitude of the spacecraft, one can integrate (10) in order to have the time evolution of the attitude.

II. Modeling Approach

Fig. 1 shows the architecture of the micropropulsion system used in the modeling that comprises: 1) a tank to store the liquid propellant (water) pressurized with nitrogen; 2) a solenoid valve to control the flow of liquid inside the thruster; 3) a MEMS resistojet with integrated heaters for the vaporization and temperature estimation; and 4) sensors for pressure and temperature measurement. The pressure sensors are placed in the tank and right before the thruster's inlet to measure the upstream and downstream pressures. The latter is the same as the chamber pressure. The temperature sensors are placed close to the nozzle which is the most suitable position due to the size of the thruster. The design of the MEMS resistojet is described in [8].

The dynamics of the system is basically governed by two factors: an unbalance between the three mass flow rates indicated in Fig. 1 contributes to the pressure changes inside the vaporization chamber and the power applied to the heaters affects the vaporization process, thus the vaporization rate and the vapor quality. As the mass flow rates considered are in terms of milligrams per second, we assume that the changes in the mass of propellant do not influence the spacecraft dynamics. The valve is used to control the mass flow rate $\dot{m}_1$ affecting the pressure inside the thruster $p_1 = p_d$ which, in turn, affects the mass flow rate $\dot{m}_3$. The vaporization rate $\dot{m}_2$ is affected by changes in pressure that change the boiling point of the propellant and by changes in the applied power that change the temperature of the thruster affecting the heat transfer to the fluid.

In order to model this dynamics, we divided the model of the microthruster into four parts: the nozzle model that provides the mass flow rate $\dot{m}_3$ based on the pressure in the chamber, the vaporization model that calculates the volumetric fraction of vapor inside the chamber, the pressure model that calculates the pressure inside the chamber based on the density of the vapor part, and the temperature model that relates the thruster temperature to the applied power.

The model of the solenoid valve combines the models of three subsystems: the electromagnetic subsystem that models the electromagnetic force generated by the solenoid, the fluidic subsystem that models the flow through the valve, and the mechanical subsystem that models the motion of the plunger. Finally, the tank is modeled as a pressurized container that reduces its pressure with the ejection of liquid and expansion of the pressurant gas.

In the system considered in this analysis, as already mentioned, there are four identical thrusters and each one has its own valve. The propellant tank, however, is shared by all the thrusters.

A. Operational Boundaries and Requirements

The models presented in this brief are developed to work within some operational boundaries set based on the requirements commonly applied to CubeSats and PocketQubes. Propulsion systems for these spacecraft usually are at a development stage that does not require strict performance parameters. Therefore, the applicable requirements regard electrical and/or mechanical constraints and safety constraints to not endanger the mission.

The maximum thrust has been estimated considering a scenario where the center of mass of the spacecraft is at most 2 cm off of the geometric center [4]. Then, the maximum thrust is calculated based on the maximum torque that the reaction wheels of the spacecraft can provide and the torque generated by a thruster positioned at the center of the furthest face of the spacecraft and pointing toward the geometric center. For a three units CubeSat with a reaction wheel that can provide 2×10^{-3} Nm, it represents a maximum thrust of 10×10^{-3} N. As a PocketQube is about eight times smaller in mass than a CubeSat, the maximum thrust is one eighth of that of a CubeSat: 1.25×10^{-3} N.

B. Vaporizing Liquid Microthruster

1) Nozzle Model: To model the mass flow rate at the nozzle $\dot{m}_3$, the ideal rocket conditions are assumed [9, p. 46]. In reality, the following assumptions of the ideal rocket theory do not apply to the microthruster considered in this brief.

1) *Adiabatic Flow:* The flow is not adiabatic since the nozzle is heated up together with the complete thruster, and therefore, there is heat transfer from the nozzle to the gas.
2) *Negligible Friction:* The friction and boundary layer effects are not negligible due to the size of the thruster.
3) *Uniform Distribution:* The gas velocity, pressure, temperature, and density are not uniform across any section normal to the nozzle axis due to friction and boundary layer effects.

Nonetheless, we assume that the changes generated by these effects can be neglected in order to simplify the modeling. Then, the mass flow going through the nozzle is given by (3). The second and third assumptions might be compensated by multiplying the mass flow rate by a discharge coefficient that can be experimentally measured for the specific device [11].

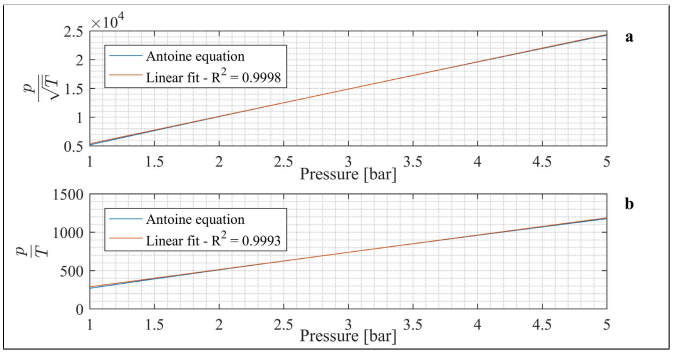

Fig. 3. Linear approximation of the pressure and temperature terms used in the modeling considering 401 points calculated using (11).

As the propellant is boiling inside the chamber, we assume that the temperature of the gas is the saturation temperature. With this assumption, the temperature of the vapor can be calculated based on the pressure using (11) known as the Antoine equation

$$T = \frac{B}{A - \log_{10} p} + C \tag{11}$$

where $A = 10.27$, $B = 1810.94$, and $C = 28.67$ for pressure in Pa and temperature in the range of 372.15–647.15 K.

If we consider the pressure in the range of 1–5 bar, then we can replace the term $(p_1/\sqrt{T_1})$ in (3) with a function of the pressure

$$\frac{p_1}{\sqrt{T_1}} = \frac{p_1}{\sqrt{\frac{B}{A-\log_{10} p_1} + C}} \approx \alpha_1 p_1 + \beta_1 \tag{12}$$

where α_1 and β_1 are the coefficients of the first-order Taylor series expansion and the functions of the parameters used in (11) and the linearization point p_s

$$\alpha_1 = \frac{C \log_{10}(p_s)^2 - (2AC+B)\log_{10}(p_s) + A(AC+B) - \frac{B}{\ln(10)}}{\left(C + \frac{B}{(A-\log_{10}(p_s))}\right)^{\frac{3}{2}} (A - \log_{10}(p_s))^2} \tag{13}$$

$$\beta_1 = \frac{p_s}{\sqrt{C + \frac{B}{(A-\log_{10}(p_s))}}} - \alpha_1 p_s. \tag{14}$$

Finally, we can rewrite (3) as follows:

$$\dot{m}_3 = (\alpha_1 p_1 + \beta_1) A_t \sqrt{\frac{k}{R_s}\left(\frac{2}{k+1}\right)^{\frac{k+1}{k-1}}}. \tag{15}$$

Evaluating the expressions around the middle point in the range of pressure of interest, i.e., $p_s = 3$ bar, we get $\alpha_1 = 0.048$ K$^{-(1/2)}$ and $\beta_1 = 626.99$ Pa K$^{-(1/2)}$.

The resulting linear equation is faster to solve computationally and provides a good fitting for the pressure and temperature term. Fig. 3(a) shows the comparison between the proposed linear approximation and the curve for $(p_1/\sqrt{T_1})$ with the temperature calculated using (11).

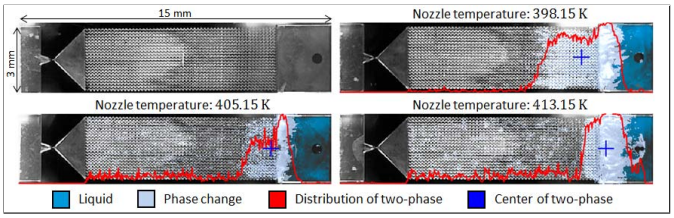

Fig. 4. Snapshots used for the measurement of the volume. An empty thruster is shown on the top-left corner for reference.

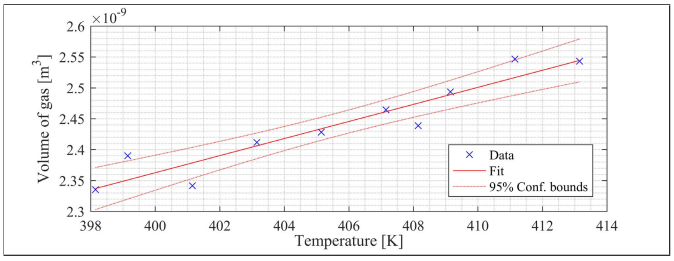

Fig. 5. Linear fitting of the volume of vapor inside the chamber as a function of the nozzle temperature for a pressure of 5 bar.

2) Vaporization Model: The vaporization rate is related to several aspects of the two-phase flow and the heat transfer that can be very difficult to measure. In order to overcome this challenge, we developed an empirical model for the change in the volume of gas inside the chamber. One of the thrusters presented in [8] was selected to undergo a series of tests to correlate the pressure and chip temperature to the volume of gas inside the chamber. Then, a linear model for the volume of gas was identified using snapshots taken during the experiments, as shown in Fig. 4. For this experiment, a digital microscope with a frame rate of 20 frames/s and a resolution of 640×480 pixels has been used.

The movement of the two-phase part is the only visible part of the propellant and is detected by taking the difference between each pixel of a frame and the same pixel of a successive frame. Then, the two-phase part of the flow is where the difference between the successive frames is higher than a certain threshold. A threshold of 80% has been empirically identified as the best value when the detected movement is similar to the movement seen with the naked eye. We can see the linear fit of the volume and the temperature in Fig. 5, where the temperatures measured at the nozzle section were ranging from 398.15 to 413.15 K for a pressure of 5 bar. Similarly, with a pressure of 3 bar, the maximum and minimum volumes were observed at the temperatures of 383.15 and 408.15 K. Then, the average volume of vapor V_{av} is written as a function of the temperature of the thruster and the pressure

$$V_{\text{av}} = a_T T_n + a_p p_1 + b \tag{16}$$

where a_T, a_p, and b are the parameters of the linear regression and T_n is the temperature of the chip measured around the nozzle. For the analysis presented here, the coefficients have been estimated as $a_T = 1.63 \times 10^{-11}$ m^3K^{-1}, $a_p = -7.45 \times 10^{-15}$ m^3Pa^{-1}, and $b = -4.36 \times 10^{-10}$ m^3.

In order to complete the model, we need an expression for the time derivative of the volume which, in this analysis, has been assumed to be a first-order linear system of the form

$$\dot{V} = A(V_{\text{av}} - V) \tag{17}$$

where $A = 75$ s^{-1} has been empirically chosen based on the image analysis already described. The rate of change in the volume is faster than the frame rate of the microscope, indicating that the time constant $\tau = (1/A)$ of a first-order system is less than 2 ms.

Then, the vaporization rate $\dot{m}_2$ can be calculated as follows:

$$\dot{m}_2 = \dot{m}_1 - \dot{V}\rho_l \tag{18}$$

where ρ_l is the density of the liquid.

3) Pressure Model: Consider the ideal gas law given by

$$\frac{p}{T}V = mR_s \tag{19}$$

where m is the mass of gas. Following a similar approach as the linear approximation used in the nozzle model, we can approximate the term (p/T) by a linear relation reducing the equation to:

$$p = \frac{1}{\alpha_2}\left(\frac{mR_s}{V} - \beta_2\right) \tag{20}$$

where

$$\alpha_2 = \frac{C\log_{10}(p_s)^2 - (2AC+B)\log_{10}(p_s) + A(AC+B) - \frac{B}{\ln(10)}}{(B - C\log_{10}(p_s) + AC)^2} \tag{21}$$

$$\beta_2 = \frac{p_s}{\sqrt{C + \frac{B}{(A - \log_{10}(p_s))}}} - \alpha_2 p_s. \tag{22}$$

Evaluating around the linearization point, one gets $\alpha_2 = 0.0023$ K^{-1} and $\beta_2 = 62.17$ $\text{Pa}\,\text{K}^{-1}$. The results of this linearization are shown in Fig. 3(b) in comparison with the values calculated using (11).

4) Chip Temperature Model: The temperature of the thruster is modeled as a linear first-order system whose input is the applied power. The Laplace transfer function of the power–temperature system is given by

$$\frac{T(s)}{P(s)} = \frac{K}{s + \frac{1}{\tau}} \tag{23}$$

where $\tau = 119.5$ s and $K = 28.5$ $\text{KW}^{-1}\text{s}^{-1}$ have been experimentally estimated using data of power and temperature.

As described in a previous research [8], the resistance used in the heaters is linearly dependent on the temperature. The change in resistance due to changes in the temperature is described by the following equation [12]:

$$R = \alpha R_0(T - T_0) + R_0 \tag{24}$$

where R is the resistance, T is the current temperature, and R_0 is the resistance measured at temperature T_0. The value of α has been experimentally characterized for many devices, and on average, it is $\alpha = 1.09 \times 10^{-3}$ K^{-1} [8].

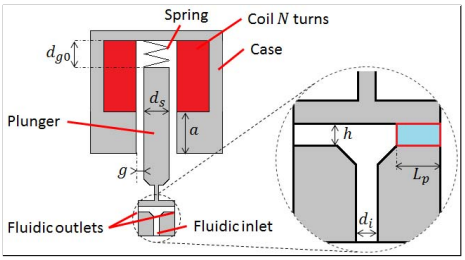

Fig. 6. Reference geometry of the valve model. The part highlighted in blue is the parallel plates section used in the fluidic model. The top edge of the plunger moves up and down and the flow goes from left to right.

C. Valve

The analytical model of a solenoid-actuated microvalve is a complex system that can be described by interfacing three different physical systems: the electromagnetic, the fluidic, and the mechanical system.

1) Electromagnetic System: The electromagnetic actuation of the valve takes place when a voltage is applied to the inner coil of the microvalve. The current flowing in the coil generates a magnetic field that pulls the magnetic plunger and consequently opens the microvalve. The equivalent electric circuit can be described by the following equation [13]:

$$v = R_c i + \dot{\lambda} \tag{25}$$

where v is the voltage, R_c is the coil equivalent resistance, i is the electric current, and λ is the flux linkage. The flux linkage is defined as $N\Phi$, where Φ is the magnetic flux. In order to express the flux linkage, a simple representation of the magnetic circuit is required, assuming that the solenoid is operating in the linear region. The electromagnetic circuit can be represented as follows according to [13]:

$$Ni = \Phi\mathcal{R} \tag{26}$$

where N is the number of turns in the coil, Φ is the magnetic flux, and $\mathcal{R}$ is the global magnetic reluctance of the circuit. The latter can be determined by geometric considerations only (see Fig. 6), regardless of the material used in the valve, since the magnetic reluctance of the air gaps is prominent with respect to that of the metallic structure.

Rearranging (25) and (26), the flux linkage can be expressed as

$$\lambda(x,i) = \frac{N^2\mu_0 A_{\text{sol}} a}{a(d_{g0}-x) + \frac{d_{\text{sol}} g}{4}} i \tag{27}$$

where μ_0 is the air permeability constant, A_{sol} is the cross section area of the solenoid, a is the bottom iron strips length, d_{g0} is the initial air gap between the plunger and the iron core, d_{sol} is the solenoid diameter, and g is the side air gap between the plunger and the iron core.

The partial derivative of the flux linkage with respect to the electric current is the equivalent magnetic inductance L of the system, which depends on the position x of the plunger. The derivative of the current in time can thus be expressed as

$$\dot{i} = \frac{1}{L(x)}(v - i(R_c + \dot{x}\dot{L}(x))) \tag{28}$$

which represents the first-order differential equation of the transient behavior of the electric current. The magnetic force that is generated by the current can be derived from the coenergy, defined as the integral of the flux linkage against the current [13]

$$F_{\text{mag}} = \frac{\partial}{\partial x}\left(\frac{L(x)}{2} i^2\right) \tag{29}$$

where F_{mag} is the magnetic force and L is the inductance of the system.

2) Fluidic System: The fluid flow within the microvalve is usually described by the orifice equation. Nevertheless, such an equation is not appropriate to simulate correctly the transient behavior rapidly occurring during the microvalve actuation. For this reason, a novel approach has been developed to include the unsteady characterization of the fluid flow. Assuming the flow occurring between two infinite parallel plates, as shown in Fig. 6 by the section highlighted in blue, the Navier–Stokes equations can be rearranged to obtain the following equation describing the time derivative of the flow bulk velocity:

$$\dot{u} = -\frac{12\mu}{\rho h^2} u + \frac{\Delta p}{\rho_l L_p} \tag{30}$$

where u is the velocity of the fluid, μ is the dynamic viscosity of the fluid, h is the height of the section, and L_p is the length of the section. The flow is considered incompressible, isothermal, and unidirectional. It is important to note that the pressure drop is that of the parallel plates region, hence different from the pressure drop across the microvalve. The pressure loss can be calculated by geometrical considerations using a numerical analysis or by the discharge coefficient of the real hardware.

The outlet volumetric flow rate Q, and hence the mass flow rate, can be calculated from the outlet velocity u and area A_{out} which is a function of x

$$Q = uA_{\text{out}}(x). \tag{31}$$

The inlet fluid flow is deviated by the plunger toward the outlet aperture; in turn, the fluid flow exerts a load on the plunger itself. The fluid force can be described using the momentum conservation of the Reynolds transport theorem

$$F_{f,\text{pl}} = p_{\text{in}} A_{\text{in}} + \rho u^2 A_{\text{in}} - \rho_l \dot{Q}(x)(x + L_0) \tag{32}$$

where $F_{f,\text{pl}}$ is the fluid force on the plunger, p_{in} is the inlet pressure, A_{in} is the inlet area, and L_0 is the minimum height of the control volume. The first two terms represent the steady-state load, whereas the third term is linked to the transient load; nevertheless, simulations have shown that its influence is negligible.

3) Mechanical System: The motion of the plunger is driven by several external loads. The main contribution is certainly given by the electromagnetic force in (29) . Its dynamics can be described by Newton's second law as follows:

$$M\ddot{x} + c\dot{x} + k(x - x_0) = F_{\text{mag}} + F_{f,\text{pl}} - p_{\text{out}} A_{\text{in}} \tag{33}$$

where M is the mass of the plunger, c is the viscous coefficient, k is the elastic constant of the spring, and x_0 is the spring preload.

4) State-Space Model: Based on the equations developed in Sections II-C1–II-C3, the state-space model can be expressed using the plunger position $x = x_1$, the plunger velocity $v = x_2$, the electric current $i = x_3$, and the fluid outlet velocity $u = x_4$ as state variables, and $y = \dot{m}_1$ the output of the system

$$\dot{x} = \begin{cases} x_2 \\ \dfrac{1}{M}(-cx_2 - k(x_1 - x_0) + F_{\text{mag}} + F_{f,\text{pl}} - p_{\text{out}}A_{\text{in}}) \\ \dfrac{1}{L(x_1)}(v - x_3(R_c + x_2\dot{L}(x_1))) \\ -\dfrac{12\mu}{\rho x_1^2}x_4 + \frac{\Delta p}{\rho L_p} \end{cases} \tag{34}$$

$$y = \rho x_4 A_{\text{out}}(x_1). \tag{35}$$

The presented state-space model fully describes the dynamics of the actuation of the solenoid-actuated microvalve.

D. Tank

The propellant tank is a pressurized tank containing a given fraction of liquid propellant, in our case water, with mass m_l. During operations, the propellant is ejected at a rate $\dot{m}_1$ and the pressurant gas, and in our case N_2, it expands lowering the pressure of the tank p_t. As the expansion is quasi-static, it can be considered an isothermal process. From the ideal gas law, the derivative of the pressure is calculated by the following equation, where V_t is the tank volume:

$$\dot{p}_t = -p_t \frac{\dot{m}_1}{V_t\rho_l - m_l}. \tag{36}$$

III. Model Analysis

A sensitivity analysis was performed in order to assess the impact of all the parameters in the response of the model. The performance parameters, such as thrust F and specific impulse I_{sp}, are the basis for the analysis. Here, we focus on the parameters that cannot be tuned by design, e.g., the estimated parameters α_1 and β_1, but instead, they depend on the operational range used or the experimental setup. Thus, as the propellant tank has been modeled using only an analytical expression to relate the mass flow rate and the pressure, it has not been covered by the sensitivity analysis, because its parameters are dependent on the specific design choices.

A. Sensitivity Analysis: Thruster

The parameters of the thruster model are shown in Table I. The sensitivity analysis has been carried out assessing all combinations of the maximum and minimum values for each parameter. These values are selected based on the boundaries defined for the model and the confidence intervals of the linearization. The outputs of the model for each set of parameters are compared to the reference outputs calculated with the reference values. The deviation of the output from the reference is the cost function of the analysis and the rank correlation values between the change in the output and the variable are given in Table II.

TABLE I
List of Input Parameters for the Sensitivity Analysis

Thruster model					
Par.	Description	Min.	Ref.	Max.	Scale/Unit
a_T	Vap. model	1.62	1.63	1.64	$10^{-11}\,\text{m}^3\,\text{K}^{-1}$
a_p	Vap. model	-7.56	-7.45	-7.33	$10^{-15}\,\text{m}^3\,\text{Pa}^{-1}$
b	Vap. model	-5.20	-4.36	-3.52	$10^{-10}\,\text{m}^3$
A	Vap. model	70	75	80	$1\,\text{s}$
α_1	Noz. model	0.046	0.048	0.05	$1\,\text{K}^{-\frac{1}{2}}$
β_1	Noz. model	197.22	626.99	1075.32	$1\,\text{Pa}\,\text{K}^{-\frac{1}{2}}$
α_2	Pres. model	0.0021	0.0023	0.0025	$1\,\text{K}^{-1}$
β_2	Pres. model	20.43	62.17	104.29	$1\,\text{Pa}\,\text{K}^{-1}$
τ	Temp. model	100	120	140	$1\,\text{s}$
K	Temp. model	25	30	35	$1\,\text{K}\,\text{W}^{-1}\,\text{s}^{-1}$
Valve model					
Par.	Description	Min.	Ref.	Max.	Scale/Unit
L_p	See Fig. 6	0.90	1.00	1.10	10^{-3}m
d_i	See Fig. 6	0.90	1.00	1.10	10^{-3}m
d_s	See Fig. 6	4.50	5.00	5.50	10^{-3}m
N	Num. of turns	27.9	31.0	34.1	1
R_c	Eq. coil res.	0.90	1.00	1.10	$10^3\Omega$
a	See Fig. 6	3.60	4.00	4.40	10^{-3}m
d_{g0}	See Fig. 6	2.25	2.50	2.75	10^{-3}m
g	See Fig. 6	2.70	3.00	3.30	10^{-4}m
M	Plunger mass	7.20	8.00	8.80	10^{-4}kg
c	Viscous coef.	450.0	500.0	550.0	$1\,\text{N}\,\text{s}\,\text{m}^{-1}$
k	Spring coef.	12.15	13.50	14.85	$10^3\text{N}\,\text{m}^{-1}$

TABLE II
Results of the Sensitivity Analysis. Values Correspond to the Rank Correlation Between the Parameter and the Output

Thruster			Valve	
Par.	Thrust	Specific impulse	Par.	Mass flow rate
β_1	0.625	0.747	N	0.055
β_2	0.115	0.088	R_c	-0.052
α_1	0.108	0.048	c	-0.051
α_2	-0.106	0.011	d_{g0}	-0.049
τ	0.085	0.091	k	-0.046
K	0.075	0.092	L_p	-0.044
b	-0.066	-0.010	g	-0.039
A	-0.066	0.045	d_s	-0.038
a_p	0.018	0.042	M	-0.023
a_T	0.006	0.027	d_i	-0.011
			a	-0.008

As we can see in Table II, the most influent parameter of the thruster model is β_1 as it has the largest correlation to the thrust and the specific impulse. The difference in the response of the model using the worst set of parameters, i.e., the ones that give the response with the largest difference to the reference response, is around 2.8% for specific impulse and 0.1% for thrust.

B. Sensitivity Analysis: Valve

An analysis similar to one of the thrusters has been done for the valve model using the parameters shown in Table I. A more detailed analysis can be found in [14] where an optimal set of parameters for the valve model has been identified comparing with experimental data. We use a range of $\pm 10\%$ around the values presented in that reference for each parameter in order to assess the influence on the mass flow rate (response of the model). All the combinations of the maximum and minimum values are used in the sensitivity analysis.

TABLE III
PARAMETERS USED IN THE SIMULATIONS

	Par.	Value	Unit	Description
Valve	M	8×10^{-4}	kg	Plunger mass
	k	1.35×10^{4}	$\mathrm{N\,m^{-1}}$	Spring constant
	c	500	$\mathrm{N\,s\,m^{-1}}$	Fluid visc. damp.
	V	12	V	Coil voltage
	R_c	31	Ω	Coil resistance
	d_{in}	0.001	m	Inlet diameter
	N	1000	1	Number of turns
	f_{PWM}	200	Hz	PWM frequency
Tank	p_{t0}	5	bar	Initial pressure
	m_{l0}	30×10^{-3}	kg	Init. mass of prop.
	V_t	40×10^{-6}	$\mathrm{m^3}$	Volume
Thruster	A_t	2×10^{-9}	$\mathrm{m^2}$	Throat area
	V_{tot}	4×10^{-9}	$\mathrm{m^3}$	Chamber volume
	α	1×10^{-3}	$\mathrm{K^{-1}}$	Temp. res. coef.
Spacecraft	h	0.15	m	Height
	w	0.05	m	Width
	l	0.05	m	Length
	m	0.5	kg	Mass
Fluid	γ	1.33	1	Ratio of spec. heat
	R_s	461.5	$\mathrm{J\,kg^{-1}\,K^{-1}}$	Spec. gas constant
	μ_{H_2O}	0.001	Pa s	Viscosity
	ρ_l	1000	$\mathrm{kg\,m^3}$	Propellant density

Table II shows the correlation between each parameter and the output of the valve model, i.e., the mass flow rate. For this model, the number of turns in the coil and the resistance are the most influent. The response in the worst case changes 0.02%.

IV. Simulation Setup

A. Spacecraft Parameters

The complete model of the micropropulsion system has been used in a simulation loop to control the attitude of a picosatellite. The satellite is a three units PocketQube consisting of three units of $5 \times 5 \times 5$ cm with a mass of 0.5 kg. Considering the mass equally distributed in all dimensions, the components of the inertia matrix around the principal axis of the spacecraft are $I_1 = 1.0 \times 10^{-3}\ \mathrm{kg\,m^2}$, $I_2 = 1.0 \times 10^{-3}\ \mathrm{kg\,m^2}$, and $I_3 = 2.083 \times 10^{-4}\ \mathrm{kg\,m^2}$. The maximum thrust provided by each thruster is defined as 1.25 mN. A complete list of the parameters used in the simulations is given in Table III.

B. Controller Design

In order to control the attitude of the spacecraft, two controllers have been implemented in the simulation loop: one to calculate the torque $\vec{M}_{\text{ref}}$ necessary to execute the desired maneuver and one to control each thruster in order to produce the desired thrust F. The former also decides which of the four thrusters to use depending on the current and target attitude. A simple proportional–derivative control law is used to calculate $\vec{M}_{\text{ref}}$ [10]

$$\vec{M}_{\text{ref}} = \boldsymbol{k}_p \hat{q}_e + \boldsymbol{k}_r \vec{\omega} \tag{37}$$

where $\boldsymbol{k}_p$ and $\boldsymbol{k}_r$ are the gains of the controller in x, y, and z, and $\hat{q}_e$ is the vectorial part of the quaternion representing the error between the current and the target attitude defined as

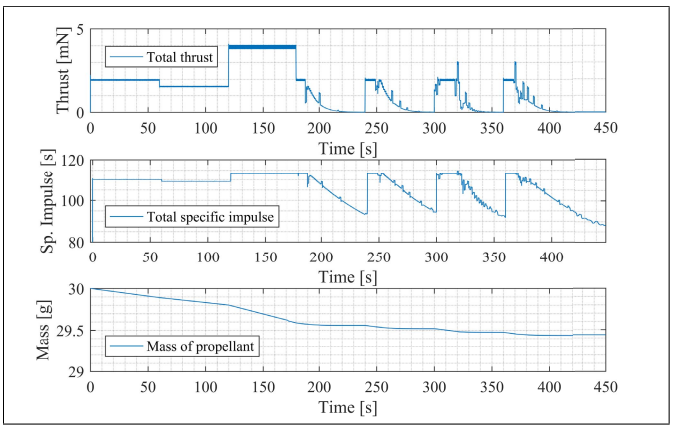

Fig. 7. Total thrust generated by the all thrusters (top), total specific impulse (middle), and mass of propellant left in the tank (bottom). The attitude control starts after 180 s.

$q_e = q^{-1} \otimes q_t$, where q_t represents the target attitude and $\otimes$ is the multiplication of two quaternions. Then, $\vec{M}_{\text{ref}}$ is used to calculate the thrust of each thruster, which is the reference input to the valve controller that actuates on the valve's input voltage $v(t)$

$$v(t) = K_p e(t) + K_i \int_0^t e(\tau) d\tau \tag{38}$$

where K_p and K_i are the gains of the controller and $e(t)$ is the error defined as the difference between the target and the actual thrust. In order to simulate the behavior of the real system, the voltage is converted into a pulsewidth modulation input with frequency f_{PWM} and amplitude V.

V. Simulation Results

The models were implemented in Simulink/MATLAB and tested in a case with four thrusters used to control the attitude of a picosatellite. The controllers were empirically tuned with the gains $\boldsymbol{k}_p = [1\ 3\ 3] \times 10^{-4}$ and $\boldsymbol{k}_r = [5\ 15\ 15] \times 10^{-4}$ for the spacecraft controller and $K_p = 200$ and $K_i = 9500$ for the valve controllers. These gains have been selected based on the desired response time, less than 0.1 s for the valves and 20 s for the spacecraft, and on the maximum allowed overshoot of less than 20% for the valves and no overshoot for the spacecraft.

The test is divided into two parts during the time of the simulation. In the first part, before 180 s, a sequence of thrust commands is sent to all the thrusters in order to assess the thrust level control. Then, after 180 s, a sequence of attitude commands is sent to the controller that calculates the necessary thrust for each of the thrusters to perform the maneuver.

Fig. 7 shows the thrust generated by all the thrusters, the total specific impulse, and the mass of propellant in the tank. The attitude angles are shown in Fig. 8 together with the commanded values shown by the red line.

As we see in Fig. 7, the mass of propellant in the tank drops very slowly, meaning that the amount of propellant considered, i.e., 30 g, can be used for a very long time before the pressure drops below a critical level where the maximum

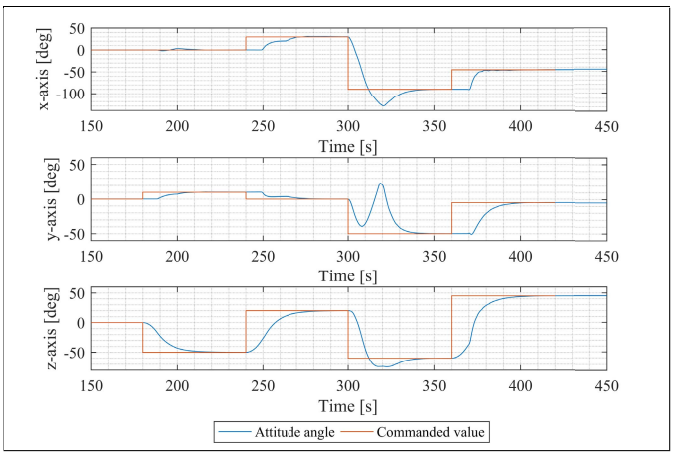

Fig. 8. Angles of the spacecraft during the attitude control phase that starts after 180 s.

provided thrust is lower than the required maximum thrust $F = 1.25$ mN.

VI. Conclusion

This brief presented a comprehensive modeling approach for micropropulsion systems using VLMs. The model developed comprises all relevant elements of microresistojets and the necessary equations to simulate the dynamics of such system. The resulting model is hybrid comprising fundamental laws of physics as well as empirical relations. Some parts of the model are derived from the well-known relations, such as the ideal gas law, and some others are empirically derived from an extensive experimental campaign done with test models of the real propulsion system. The models of the thruster, the valve, and the tank have been tuned to work within the boundaries usually considered for miniaturized spacecraft, e.g., CubeSats and PocketQubes, in terms of operational parameters, such as pressure and temperature. However, these boundaries can be changed in order to adapt and extend the model to other applications with different sets of requirements.

The model has been successfully applied in a simulation loop demonstrating the attitude control of a picosatellite using an array of four thrusters. The model can be applied in other types of simulation that need a precise description of the system dynamics, including the optimization of the propulsion system's parameters and the thruster's parameters.

All the empirical parts of the model are sufficient for the type of analysis presented here. However, a more accurate model might be achieved by using theoretical relations empirically adjusted to the conditions of the test. For example, a discharge coefficient can be applied to the nozzle model in order to account for losses. A more sophisticated vaporization model might be used to replace the volumetric change of the gas. However, as most of the models found in the literature are empirical relations derived for specific cases depending on the two-phase flow regime, a more detailed empirical model for the flow inside a resistojet might be a good choice. The gas volume model might be improved with the use of a more sophisticated test setup, including high-speed cameras to capture the motion of the fluid more precisely.

Future work will be focused on the extension of the modeling to address the points mentioned and to improve the accuracy of the model by considering a broader range of operational parameters. The comparison of the model with experimental data might further improve the validation of model which has been done only numerically. A more advanced application scenario will also be considered in order to investigate other characteristics of thrust control in micropropulsion applications.

References

[1] D. Selva and D. Krejci, "A survey and assessment of the capabilities of cubesats for earth observation," *Acta Astronautica*, vol. 74, pp. 50–68, May/Jun. 2012.

[2] K. Lemmer, "Propulsion for CubeSats," *Acta Astronautica*, vol. 134, pp. 231–243, May 2017.

[3] M. Leomanni, A. Garulli, A. Giannitrapani, and F. Scortecci, "Propulsion options for very low earth orbit microsatellites," *Acta Astronautica*, vol. 133, pp. 444–454, Apr. 2017.

[4] M. A. C. Silva, D. C. Guerrieri, A. Cervone, and E. Gill, "A review of MEMS micropropulsion technologies for cubesats and pocketqubes," *Acta Astronautica*, vol. 143, pp. 234–243, Feb. 2018.

[5] D. Maurya, S. Das, and S. Lahiri, "An analytical model of a silicon MEMS vaporizing liquid microthruster and some experimental studies," *Sens. Actuators A, Phys.*, vol. 122, no. 1, pp. 159–166, 2005.

[6] M. Bidabadi, M. Heidari, and A. Rahbari, "A novel analytical model of a MEMS vaporizing liquid micro thruster," in *Proc. 2nd Int. Conf. Comput. Automat. Eng.*, 2010, pp. 321–325.

[7] D. C. Guerrieri, M. A. C. Silva, A. Cervone, and E. Gill, "Selection and characterization of green propellants for micro-resistojets," *ASME J. Heat Transfer*, vol. 139, no. 10, p. 9, 2017.

[8] M. A. C. Silva, D. C. Guerrieri, H. van Zeijl, A. Cervone, and E. Gill, "Vaporizing liquid microthrusters with integrated heaters and temperature measurement," *Sens. Actuators A, Phys.*, vol. 265, pp. 261–274, Oct. 2017.

[9] G. P. Sutton and O. Biblarz, *Rocket Propulsion Elements*, 8th ed. Hoboken, NJ, USA: Wiley, 2010.

[10] B. Wie and P. M. Barba, "Quaternion feedback for spacecraft large angle maneuvers," *J. Guid., Control, Dyn.*, vol. 8, no. 3, pp. 360–365, 1985.

[11] S. Janson, H. Helvajian, and K. Breuer, "Mems, microengineering and aerospace systems," in *Proc. 30th Fluid Dyn. Conf.*, 1999, p. 3802.

[12] L. Mele *et al.*, "A molybdenum MEMS microhotplate for high-temperature operation," *Sens. Actuators A, Phys.*, vol. 188, pp. 173–180, Dec. 2012.

[13] N. C. Cheung, K. W. Lim, and M. F. Rahman, "Modelling a linear and limited travel solenoid," in *Proc. Int. Conf. Ind. Electron., Control, Instrum.*, 1993, pp. 1567–1572.

[14] S. Silvestrini, "Closed-loop thrust magnitude control system for nano- and pico-satellite applications," M.S. thesis, Fac. Aerosp. Eng., Delft Univ. Technol., Delft, The Netherlands, 2017.